

Improvements on the third generation of electron momentum spectrometer*

Ning Chuan-Gang(宁传刚), Zhang Shu-Feng(张书锋), Deng Jing-Kang(邓景康)[†],
Liu Kun(刘 昆), Huang Yan-Ru(黄艳茹), and Luo Zhi-Hong(罗志弘)

*Department of Physics and Key Laboratory of Atomic and Molecular NanoSciences of Ministry of Education,
Tsinghua University, Beijing 100084, China*

(Received 22 June 2007; revised manuscript received 12 November 2007)

The significant modifications to our recently constructed electron momentum spectrometer have been implemented. Compared with our previous report, the energy and the angle resolutions are significantly improved and reach $\Delta E = 0.45$ eV, $\Delta\theta = \pm 0.53^\circ$ and $\Delta\phi = \pm 0.84^\circ$, respectively. Moreover, the details of data reduction and the relation between azimuthal angle range and the sensitivity are discussed.

Keywords: electron momentum spectrometer, double toroidal analyser, oxide cathode, Monte Carlo simulation

PACC: 3480G

1. Introduction

The electron momentum spectroscopy, also known as binary (e, 2e) spectroscopy, has been developed as a powerful tool for studying electronic structures and correlation effects of matter. The ability to measure the electron density in momentum space, the squared modulus of a momentum-space wave function, is a remarkable feature of this technique.^[1–5] The first successful electron momentum spectroscopic (EMS) experiments were reported over 30 years ago with an energy resolution of about 64 eV and a momentum resolution of about 2 a.u. for thin film targets.^[6,7] It was at about the same time that the EMS measurements of gas targets with much improved energy and momentum resolutions were reported.^[8] This study on argon showed for the first time both the ability for EMS to map the momentum densities of target electrons for individual transition and the importance of correlation effects in the inner valence region. Used in these seminal studies were single energy channel and single angle channel measurements due to the limitation of detection techniques at that time. This single point measurement mode is one of the characteristics of the first generation spectrometer (EMS-1). Since all the experimental conditions needed for EMS lead to quite small cross sections,^[3] the earlier EMS re-

sults always suffer from a large statistical uncertainty and a low energy resolution. In order to overpass this obstacle, it is necessary to develop multi-channel electron detection techniques that allow for the simultaneous measuring of series of energies or angles (i.e. momenta). Pioneered by Moore *et al.*^[9] a spherical analyser equipped with an array of channel electron multipliers was used to simultaneously measure a series of azimuthal angles. Thereafter, Weigold *et al.*^[10] have introduced one-dimensional position-sensitive detectors (PSDs) for parallel measurements over a range of energies. Brion *et al.*^[11] have reported a momentum dispersive spectrometer. These spectrometers are either energy or momentum dispersive and can be roughly classified as the second generation (EMS-2). Most of the second generation of spectrometers adopt the hemispherical analysers (HSA) to realize the energy multi-channel measurement.^[11–17] HSA has a simple structure but with excellent performances and it is also widely used in other types of spectrometers, such as photoelectron spectrometer (PES). With HSA, Brunger *et al.*^[18,19] reported a high-resolution EMS-2 spectrometer. Although a great many of impressive results have been achieved on EMS-2 spectrometers, the low coincidence count rate and the long measuring time have greatly restricted the application of EMS to small stable molecules. Recently, with

*Project supported by the National Natural Science Foundation of China (Grant No 10575062) and Specialized Research Fund for the Doctoral Program of Higher Education of China (Grant No 20050003084).

[†]E-mail: djkdmp@mail.tsinghua.edu.cn

the development of novel smart electron energy analysers and large size PSDs, several groups reported their third generation of EMS spectrometers (EMS-3),^[1,20–24] which can execute energy multi-channel as well as angle multi-channel measurements. And, recently, Takahashi *et al*^[25] reported a seminal (e, 2e) experimental investigation for oriented molecules. Most of those spectrometers take a non-coplanar symmetrical geometry in which a full 2π azimuthal angle range can be attained for both outgoing electrons with only one analyser.^[1,22,23] These spectrometers with the non-coplanar symmetrical geometry can significantly improve the coincidental count rates by using a large azimuthal angle range, the resolutions, however, have not been evidently improved.

Some significant modifications to our recently constructed EMS-3 spectrometer have been made to improve its resolutions. This spectrometer has a non-coplanar symmetrical geometry and is equipped with a double toroidal analyser to realize parallel detection of energies and angles of electrons. The design of spectrometer is optimized by using the Monte Carlo simulation of electron optics, so the performance of the spectrometer, especially its momentum resolution, is significantly improved. An electron gun equipped with an oxide cathode, which works at a much lower temperature than the generic filament cathodes, is used to generate the electron beam with a low energy spread and a low divergence angle.

EMS for directly measuring the electronic structures of matter is straightforward conceptually. In (e, 2e) spectrometer a high-energy incident electron knocks out an electron from the target and the two outgoing electrons are subsequently detected in coincidence. Measuring the incident electron momentum p_0 , and two outgoing electron momenta p_1 and p_2 allows the target electron binding energy, ε , and the target recoil electron momentum, q , to be determined by using the conservations of energy and momentum:

$$\varepsilon = E_0 - E_1 - E_2, \quad (1)$$

$$q = p_0 - p_1 - p_2. \quad (2)$$

At high energy and high momentum transfer $K = |p_0 - p_1|$, the (e, 2e) collisions involve clean knocking out of the target electron, and the recoil momentum is equal in magnitude but opposite in direction to the momentum of the struck target. With a non-coplanar symmetrical geometry, the two outgoing electrons have the same kinetic energies and the same polar angles, i.e. $E_1 \approx E_2$, $\theta_1 = \theta_2 = 45^\circ$, and $p_1 \approx p_2$,

and the momentum p can be given by

$$p = \left\{ (2p_1 \cos\theta_1 - p_0)^2 + [2p_1 \sin\theta_1 \sin(\phi/2)]^2 \right\}^{1/2}, \quad (3)$$

where $\phi = \phi_2 - \phi_1$ is the azimuthal angle relative to the scattering plane with ϕ_1 and ϕ_2 being the azimuthal angles relative to the middle lines of the electron detectors. Under sufficiently high electron energy and momentum transfer, the (e, 2e) cross section for a randomly oriented gas target can be written as

$$\sigma_{\text{EMS}} \propto \int \langle \nu_{\mathbf{p}} \Psi_{\mathbf{f}}^{N-1} | \Psi_{\mathbf{i}}^N \rangle^2 d\Omega, \quad (4)$$

where $\Psi_{\mathbf{i}}^N$ and $\Psi_{\mathbf{f}}^{N-1}$ are the total electronic wave functions for the N -electron target species and the $(N-1)$ electron product ion, respectively, and $\nu_{\mathbf{p}} = e^{i\mathbf{p}\cdot\mathbf{r}}$ is a plane wave representing the target electron at the collision instant. The overlap between the neutral ground state and ionized states, $\langle \nu_{\mathbf{p}} \Psi_{\mathbf{f}}^{N-1} | \Psi_{\mathbf{i}}^N \rangle$, is also known as Dyson orbital, which can be calculated with Configuration interaction (CI)^[26] and Green's function (GF)^[27] theories. Under the target Hartree–Fock (HF) or Kohn–Sham (KS) approximations, the measured electron momentum distributions reduce to structure factors derived as the square of HF or KS orbitals in their momentum representation.^[3] Therefore, EMS is very commonly regarded as a powerful orbital-imaging technique.

2. Design criteria

The electron momentum spectrometer requires a suitable electron beam source, a target, an electron analyser, and a detection system for two outgoing electrons. The electron beam source provides a well-collimated, low energy spread electron beam with an energy of E_0 for ionizing the target. The detection system must provide the energy-, angle-, and time-resolved coincident detection for two outgoing electrons from (e, 2e) events with a high resolution. The time-resolved detection allows the true coincidence event to be determined by subtracting random background events. Another important criterion of design is the high sensitivity, so the solid angle for collecting electrons should be as large as possible. In order to reach these goals, considerable efforts have been made over last three decades. Here we report our high-resolution EMS-3 spectrometer in detail.

2.1. Electron optics

Our EMS-3 spectrometer uses the non-coplanar symmetrical geometry because such a geometry has a distinct advantage that the two outgoing electrons can share one analyser. As Fig.1 shows, a polar angle of 45° is chosen to match the Bethe ridge condition.

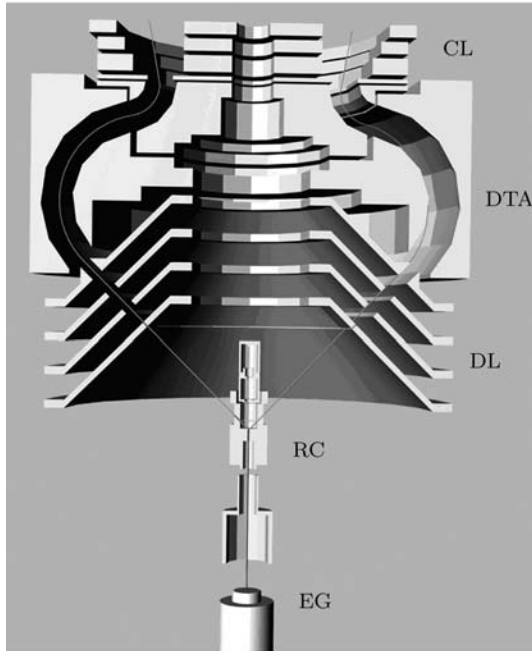


Fig.1. Schematic diagram of the energy and angular multi-channel electron momentum spectrometer, showing electron gun (EG), reaction chamber (RC), deceleration lens (DL), double toroidal analyser (DTA), and correction lens (CL). The trajectories illustrate the flight routes of two outgoing electrons from one ($e, 2e$) event.

Most of EMS-3 spectrometers take this advantage to obtain a large acceptance range of the azimuthal angle, and, with this geometry, it is possible to realize a detection range of a full azimuthal angle (2π). To achieve the high resolution energy and angle analysing power, a double toroidal analyser (DTA) is chosen in our EMS-3 spectrometer. As demonstrated in Refs.[28–32], the DTA equipped with a conical decelerating lens can realize the high energy resolution and high luminosity simultaneously. However, the azimuthal angle resolution is not satisfactory in our previous design.^[1,33–37] With a systematical Monte Carlo simulation of the electron optics of our EMS-3 spectrometer, the azimuthal angle resolution is found to be

$$\Delta\phi_1 = kd/r, \quad (5)$$

where d is the diameter of the incident electron beam, and r is the hitting position on the detector away from the symmetry axis of spectrometer, and the coefficient k depends on the potential of electron optics and the flight distance. It is obvious that the smaller the value of d is, and the larger the value of r is, the better the resolution of ϕ will be. The second stage of DTA incorporated with correction lens makes r as big as possible, and the median value of r is 46 mm in the design. It is easier to realize a small d by using an aperture hole. As Monte Carlo simulations show in Fig.2, the values of (full width at half maximum (FWHM)) $\Delta\phi_1$, are 0.45° , 1.2° and 1.7° correspond to the values of the electron beam diameter d are 0.1 mm, 0.3 mm and 0.5 mm respectively. Moreover, a smaller electron beam size also implies a better energy resolution as simulations indicated. In aforementioned simulations, the electron energy E_0 is 600 eV and the passing energy is 50 eV. A molybdenum aperture with a hole of 0.3 mm in diameter is finally used to constrain the incident electron beam size.

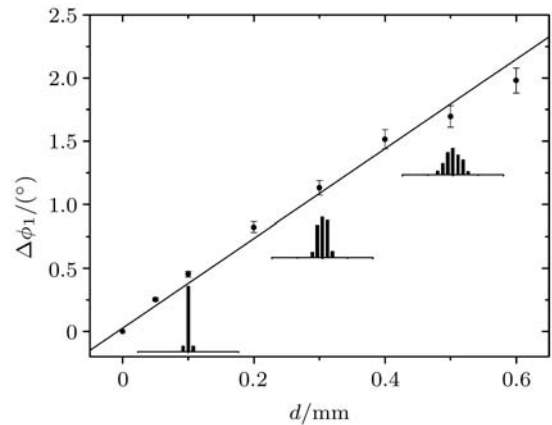


Fig.2. The azimuthal angular resolution versus the size of electron beam. The histograms are the results of the Monte Carlo simulation with 500 samples for electron beam sizes: 0.1, 0.3, and 0.5 mm, shown in sequence. The scale bars for the histograms are 10° .

2.2. Electron beam source

The crucial step in improving the energy resolution of EMS spectrometer is to produce an electron beam with a low energy spread. The widely used electron gun equipped with a thoriated tungsten filament has an energy spread of about 0.6 eV due to its high working temperature. Moreover, a voltage drop due to the resistance of filament is another important source of energy uncertainty. Most oxide cathodes can work

at a much lower temperature, typically 1100 K, correspondingly, with an energy spread of 0.3 eV, and the indirect heating mode may be free from the resistance voltage drop. However, most of oxide cathodes are prone to poisoning, i.e. its power of emitting electrons will significantly decline, and they even completely stop working, by active gas, such as O₂. To solve this problem, an additional vacuum chamber is designed in which an electron gun is mounted. This chamber is evacuated to a pressure of 10⁻⁷ Pa by a 600 L/s molecular turbopump, and it has a 2 mm diameter hole connected to the main chamber, so that electron beam can enter the main chamber through the hole. This differential evacuation stage can maintain the electron gun chamber at 8 × 10⁻⁷ Pa when main chamber is at 4 × 10⁻⁴ Pa as the gas sample is inlet to the reaction chamber. It is found that besides the working temperature of cathodes, the space charge effects can also significantly broaden the energy spread of electron beam. The spread of elastically scattering electron energy is remarkably broadened from 0.35 to 0.50 eV (FWHM) as the emitting current increases from 1 to 9 μA. It should be noted that the collected current by a faraday cup in the rear of the reaction region is only about 15% of the emitting current of the cathode due to the 0.3 mm small hole in the front of the reaction region. An electron gun, which can produce electron beams with a small beam size, a low divergence angle and a low energy spread, is highly expected.

2.3. Electronics

Two wedge strip type PSDs^[38] with a sensitive area of 50 mm in diameter are used to detect electrons in our spectrometer. The electronics for data acquisition is similar to that used in our EMS-2 spectrometer.^[39] The charge division method can provide a very good ratio of signal to noise but the signals are rather slow, therefore there appear pulse pile-ups due to the high count rate, typically 10 k/s. Considering the high count rate of EMS-3 spectrometer, the multi-parameter acquisition system is extended with a pile-up rejector. The shaping time constants of the amplifiers are set to be 1 μs, while the pile-up threshold is set to be 6 μs. Contrast with the general using of the pile-up rejection signal as the anti-gate signal of ADC, which requires a peak-hold circuit to hold the peak for at least 6 μs before conversion, so that the dead time of system is significantly increased, we use

them as the veto signal of writing memory because the coincidental count rate is much lower than that of single count rate, thus almost no additional dead time appears.

3. Data reduction

3.1. Calibration of energy and angle

The first step in obtaining the energy and the angle of electrons from the hitting position on the PSD is the calibration of the analyser. Calibration of the analyser is carried out by using a set of apertures mounted on the front of the decelerating lens. Electrons leaving from the reaction region must pass through the calibration apertures before entering the optics. Elastic scattering from a gas sample provides accurate energy- and angle- calibrations of the detectors. A series of peaks corresponding to known energies and angles are collected. From the calibration, the angle resolution of ϕ_1 is known to be 1.4° (FWHM), so the standard deviation of ϕ is ±0.84°, while ±1.9° for our previous setup.^[1] This is well consistent with 1.2° of the Monte Carlo simulations when the assembling errors of all parts are considered. To obtain a high resolution momentum, the uncertainty of polar angle θ also needs to be kept as small as possible. There are contributions to $\Delta\theta$ coming from two parts: one is the pencil angle of the incident electron beam and the other is the acceptance angle of analyser. As a smaller acceptance angle leads to a smaller collecting solid angle, we mainly struggle to make a smaller pencil angle. The final uncertainty of θ is improved from ±0.7° to ±0.53° by modifying the electron gun design.

3.2. Efficiency correction

The timing spectrum is a crucial element for establishing the coincidence between two electrons detected by both detectors. To subtract the accidental contribution, two windows are set on the timing spectrum. The narrow one with counts $N_c(\varepsilon, \phi)$, and width ΔT_c , which includes the peak, corresponds to the true coincident plus the accidental coincident counts, while the broad one with counts $N_b(\varepsilon, \phi)$, and width ΔT_b corresponds to the accidental coincidental background. The true coincident $N_t(\varepsilon, \phi)$ can be given by

$$N_t(\varepsilon, \phi) = N_c(\varepsilon, \phi) - N_b(\varepsilon, \phi)/R, \quad (6)$$

where R is the ratio of two window widths, i.e. $\Delta T_b = R\Delta T_c$. To obtain the real density distribution $N_r(\varepsilon, \phi)$ of the measured sample, $N_t(\varepsilon, \phi)$ should be corrected with a response function $F(\varepsilon, \phi)$ of the spectrometer, i.e. $N_r(\varepsilon, \phi) = N_t(\varepsilon, \phi)/F(\varepsilon, \phi)$. Fortunately, $F(\varepsilon, \phi)$ is proportional to $N_b(\varepsilon, \phi)$. To control the statistical errors, it is rational to assume

$$F(\varepsilon, \phi) \propto N_b(\varepsilon)N_b(\phi), \quad (7)$$

where $N_b(\varepsilon) = \sum_{\phi} N_b(\varepsilon, \phi)$ and $N_b(\phi) = \sum_{\varepsilon} N_b(\varepsilon, \phi)$. The summations run through the measured ranges of

ε and ϕ , respectively. Scanning energies of the incidental electron beam can uniform the $N_b(\varepsilon)$. However, it is still necessary to make some corrections at both ends of scanning range; otherwise a much wider range should be scanned than the region of interest. If the count N_b has a large statistical fluctuation, some smoothing processes can be used to control the statistical errors. Figure 3 shows a response function for measuring the calibration gas argon. Each detector has an energy range of 9 eV and an azimuthal angle range of 40° .

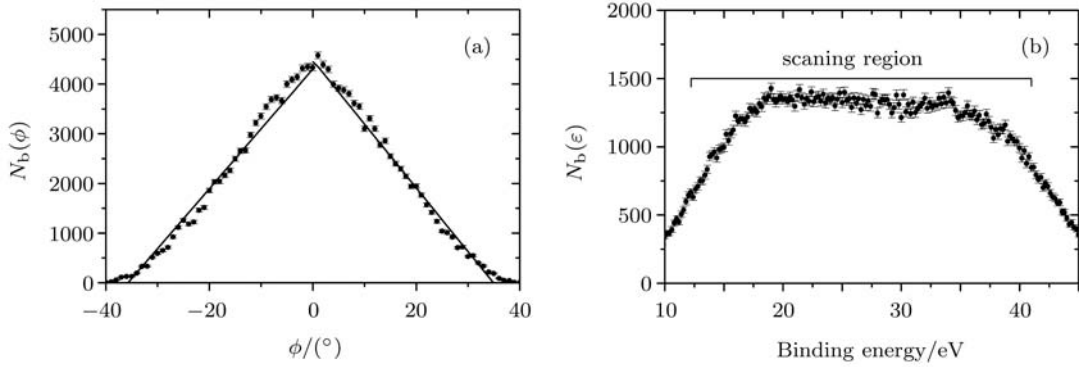


Fig.3. The efficiency function for azimuthal angle (a) and binding energy (b). The solid lines in panel (a) are the linear least square fittings. Each detector has an angle range of 40° and an energy range of 9 eV. It can be seen that correction for energy efficiency is necessary, although scanning the beam energy can uniform the efficiency in most part other than only at two ends of scanning.

The momentum resolution of an EMS spectrometer is controlled by the angular resolution of the incident and the scattered beams. The finite energy resolution can usually be ignored, and its contribution to the momentum uncertainty is less than 0.01 a.u. in most cases. However, for an energy multi-channel spectrometer, the detected energy range of 10 eV can make a significant contribution to the momentum spread. For example, a 10 eV range in energy corresponds to a momentum spread of 0.055 a.u. (full width) at an electron energy of 600 eV. If this uncertainty is not allowed for, the momentum can be accurately calculated for each (e, 2e) event because the detected energy and azimuthal angle are recorded event by event in the raw data. If the data are processed directly in momentum space, correspondingly, the response function $F(\varepsilon, p)$ can also be obtained. However, since the p depends on ε , $F(\varepsilon, p)$ proportional to $N_b(\varepsilon, p)$ cannot be simply written as $N_b(\varepsilon)N_b(p)$ any more. Moreover, the minimum value of detectable momentum p_{\min} , which is a nonzero value and depends on ε , must be carefully considered when the

boundaries of momentum bins are set. The lower boundary of first momentum bin should be p_{\min} , and $p_{\min} + ndp$ for the $(n + 1)$ th bin, where dp is the momentum interval for counting. Figure 4 shows the response function $F(\varepsilon, p)$ at $\varepsilon = 15.8$ eV versus p and at $\varepsilon = 29.2$ eV respectively. Generally, the statistical fluctuation of $N_b(\varepsilon, p)$ is quite large, we can calculate $F(\varepsilon, p)$ from $N_b(\phi)$ by using Eq.(3) with a higher accuracy. It is reasonable to assume

$$F(\phi) = 1 - \alpha |\phi|, \quad (8)$$

where α is the constant coefficient, and $0 \leq |\phi| \leq \phi_{\max}$. By using Eq.(3), we have

$$F(x; \varepsilon) = \left(1 - 2\alpha \arctg \sqrt{\frac{x^2 - x_0^2}{4 - x^2 + x_0^2}} \right) \times \frac{4x}{\sqrt{x^2 - x_0^2} \sqrt{4 - x^2 + x_0^2}}, \quad (9)$$

where

$$x = \frac{p}{p_1 \sin \theta} \quad \text{and} \quad x_0 = \frac{p_0 - 2p_1 \sin \theta}{p_1 \sin \theta}. \quad (10)$$

As $F(x; \varepsilon)$ has a singularity at $x = x_0$, it is necessary to calculate the average value in a range of $[x_0 + ndx, x_0 + (n + 1)dx]$ for comparison with the experimental data in low momentum ranges. As $x - x_0 \ll 1$, we have

$$\overline{F_n(x; \varepsilon)} \approx 2 \left(\sqrt{(n + 1)^2 + \frac{2(n + 1)x_0}{dx}} - \sqrt{n^2 + \frac{2nx_0}{dx}} \right)$$

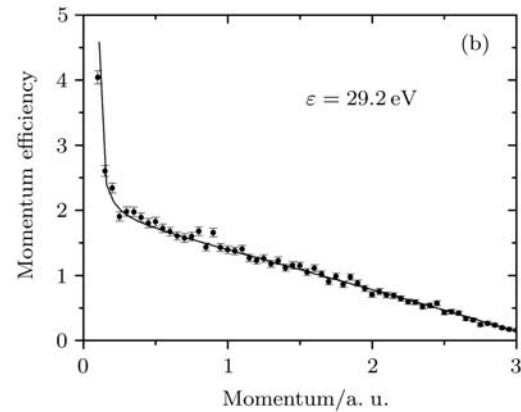
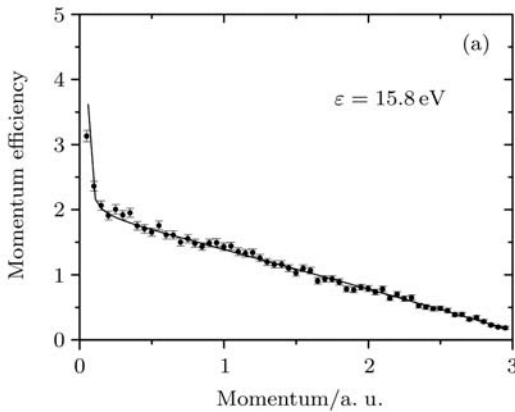


Fig.4. Momentum efficiency function for the values of binding energy ε : 15.8 (a) and 29.2 eV (b) at impact energy 1200 eV plus binding energy. The solid lines are for the results calculated from the angle efficiency and the relation between momentum p and angle ϕ . The sharp turn up in low momentum ranges is due to the nonlinear dependence of momentum p on angle ϕ . The scattering data points are the sum of accidental counts within ± 2 eV around the binding energy ε .

In order to obtain an appropriate density distribution, the potentials of electron optics must be carefully matched; otherwise, there may occur some artificial distribution among the measured results. At one time, there was always a residual background on our measured binding energy spectra. For example, there was ever a noticeable intensity between argon 3S and 3P states although we had subtracted the accidental background as aforementioned (see Fig.5 in Ref.[1]). It was obviously an artificial effect because there were not any measurable intensity distributions there in physics. Finally, it was found that this residual background problem was caused by the secondary electrons. As Fig.5 shows, some electrons hit on the correction lens after passing through the analyser, and generate secondary electrons, and then they are accelerated by field toward the multi-channel plates (MCP) because the front potential of MCP is positive relative to the correction lens. The hitting position of the secondary electrons will indicate a wrong energy value. With careful simulations, the potentials are adjusted such that the hitting from those secondary electrons

$$-\alpha dx - 2\alpha(x_0 + ndx), \tag{11}$$

where $dx = dp/(p_1 \sin \theta)$ is the experimental interval for counting in the n th bin. As the solid curves show in Fig.4, the calculations can well reproduce the $N_b(\varepsilon, p)$. The sharp turn-up in low momentum ranges is due to the nonlinear relation between p and ϕ , and its shape depends on E_0 and ε .

is avoided, and then the residual background will disappear. A typical binding energy spectrum without residual background can be found in Fig.6.

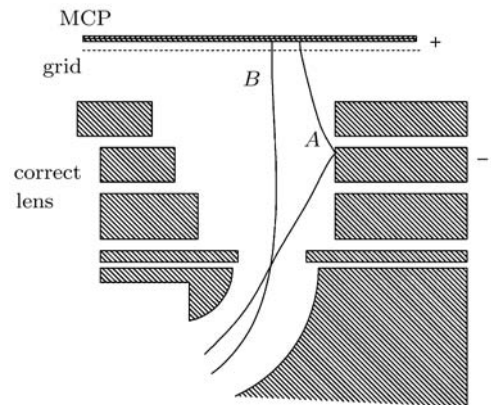


Fig.5. Mis-matched-potentials-induced residual background problem. Some electrons can be properly analysed (trajectory B), but some electrons hit on the lens (trajectory A) and produce one or more secondary electrons, which impinge on MCP due to the attracted field. If the potentials are adjusted such that the hitting from those secondary electrons is avoided, the residual background will disappear.

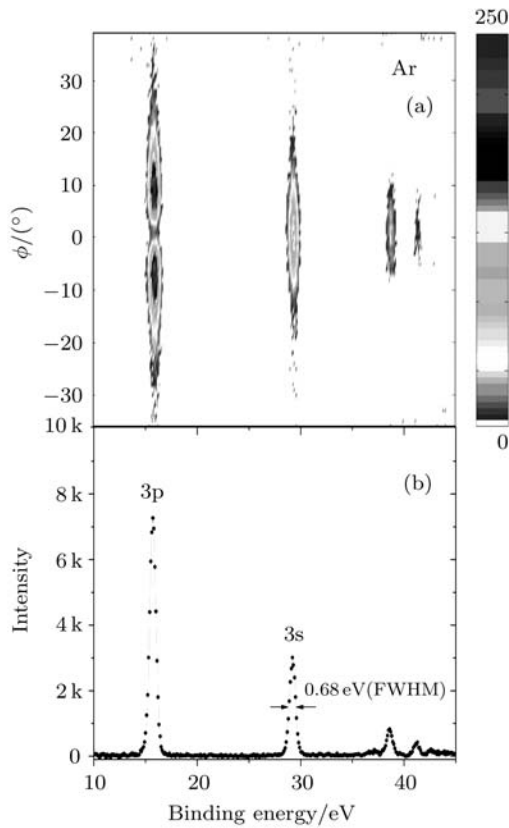


Fig.6. Directly measured EMS density map of argon (a) and intensity versus binding energy (b) with the measurement conducted at an impact energy of 1200 eV plus binding energy with a passing energy of 50 eV and an energy resolution of 0.68 eV (FWHM).

4. Results and discussion

Shown in Fig.6 is a typical experimental argon valence orbital electron density distribution versus the binding energy and the azimuthal angle (i.e. momentum), which is measured at an impact energy of 1200 eV plus binding energy with a passing energy of 50 eV. The coincidental count rate is about 12/s with a collecting current of $1 \mu\text{A}$, which is mainly limited by space charge effects. It can be seen that the instrumental energy resolution is about 0.68 eV (FWHM) in this condition. As shown in Fig.7, the ratio of peak to valley of the angle distribution for argon 3P state is about 8.5:1, while 4.3:1 in our previous report.^[1] This ratio is a directly measurable index reflecting the momentum resolution. The momentum resolution in this condition is about 0.069 a.u. (standard deviation) as the Monte Carlo momentum resolution convolution method indicated in Ref.[40]. If the emitting current decreases to $1 \mu\text{A}$, the energy resolution can be further improved to 0.45 eV with a passing energy of 30 eV. As

Fig.8 shows, the krypton $4P_{3/2}$ and $4P_{1/2}$ states can be well resolved.

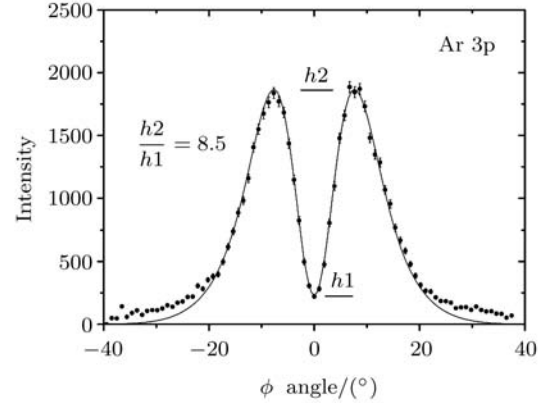


Fig.7. Angular intensity distribution for argon 3P state, showing the ratio of peak to valley, which reflects the momentum resolution of the spectrometer, to be significantly improved from 4.3:1 to 8.5:1. The solid line is for the theoretical results, and it is convoluted with $\Delta\theta = \pm 0.53^\circ$ and $\Delta\phi = \pm 0.84^\circ$ by using the Monte Carlo momentum resolution convolution method.^[40]

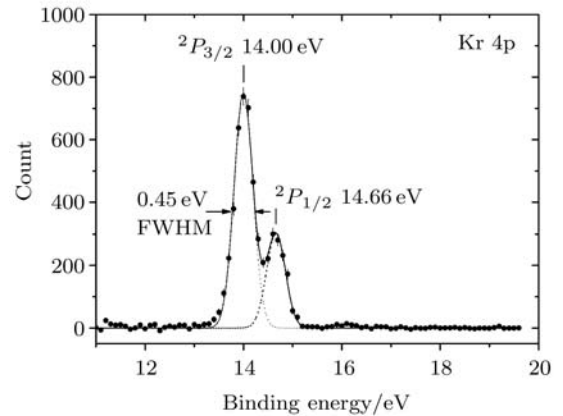


Fig.8. Binding energy spectrum of krypton 4P state, where the curves are for the two fitted Gaussian functions and their sums, with the measurement conducted at an impact energy of 1200 eV plus binding energy with a passing energy of 30 eV, and an emitting current of $1 \mu\text{A}$.

It is instructive to investigate the coincidental count rate versus the detection azimuthal angle range. It is easy to obtain such relations by setting an azimuthal angle range ϕ_R for each detector by using a software. As shown in Fig.9, the coincidental count is approximately proportional to the square of ϕ_R when $\phi_R < 20^\circ$, while linearly depends on ϕ_R when $\phi_R > 25^\circ$. The reason for this dependence is that the two outgoing electrons are angle-correlated mainly in small values of ϕ_R at an impact energy of 1200 eV for argon target. The sensitivity at $\phi_R = 30^\circ$ is about

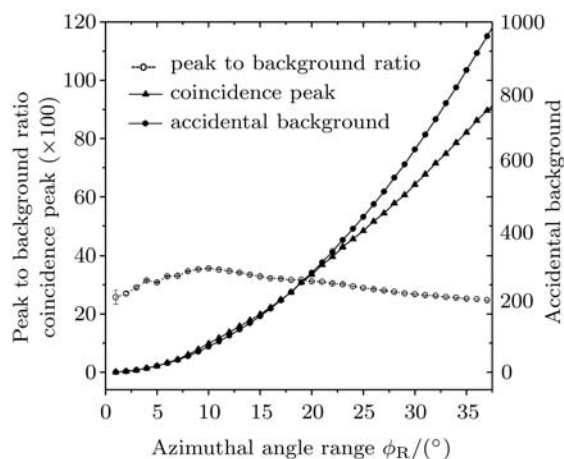


Fig.9. Coincidental peak (the left vertical axis), accidental background (the right axis) and their ratio (the left axis) versus azimuthal angle range ϕ_R for argon target. The experimental data are obtained at an impact energy of 1200 eV plus binding energy with a passing energy of 50 eV. The count of coincidental peak are the averaged values over those channels higher than half a maximum.

850 times higher than that at $\phi_R = 1^\circ$. From the trends shown in Fig.9, it can be estimated that the sensitivity will increase about 4300 times when both detectors have 100° azimuthal ranges. Therefore, the generally believed 10,000 times is overestimated due to neglecting the angle correlations. It can be seen that the accidental coincidental count, which has no angle correlations, appears to be proportional to the square of ϕ_R , thus the ratio of signal to noise (SNR) will linearly decline as ϕ_R increases for $\phi_R > 25^\circ$. Since SNR is still rather high, a large-size position-sensitive de-

tector with a fast response is still highly expected. For example, if a large size delay line detector with multi-hit ability is used to detect both outgoing electrons simultaneously,^[41] a full 2π acceptance range can be realized. These estimations have a wide applicability although they are based on the argon target because most molecules have not only s-type but also p-type orbitals in valence shell.

With this spectrometer, we hope to show that EMS can contribute to an understanding of the electronic structures as well as the (e, 2e) theories. Until now, the plane wave impulse approximation, the target Hartree–Fock approximation or the target Kohn–Sham approximation, these corner-stones of EMS, are mainly founded on the atoms or simple molecules. Although these approximations proved to be still valid for lots of complex molecules, some abnormal effects contradict these approximations^[42–47] such as the ethylene^[39] and acetone issues.^[40] Moreover, the EMS targets are mainly restricted to organic molecular systems with low Z elements at current stage. The transitional metal compounds, which are very important functional materials in our daily life, are seldom approached with EMS. For the transitional metal compounds, the correlated effects and relativistic effects are both prominent due to the high Z elements, thus it is a challenge to the theoretical treatment at current stage. Therefore, we think that the powerful EMS incorporated with the electron impact ionization theories^[48–50] can contribute significantly to an understanding of electronic structures.

References

- [1] Ren X G, Ning C G, Deng J K, Zhang S F, Su G L, Huang F and Li G Q 2005 *Rev. Sci. Instrum.* **76** 063103
- [2] McCarthy I E and Weigold E 1991 *Rep. Prog. Phys.* **91** 789
- [3] Weigold E and McCarthy I E 1999 *Electron Momentum Spectroscopy* (New York: Kluwer)
- [4] Brion C E 1986 *Int. J. Quantum Chem.* **29** 1397
- [5] Coplan M A, Moore J H and Doering J P 1994 *Rev. Mod. Phys.* **66** 985
- [6] Amaldi U, Edidi Jr. A, Marcoero R and Pizzella G 1969 *Rev. Sci. Instrum.* **40** 1001
- [7] Camilloni R, Giardini-Guidoni A, Tiribelli R and Stefani G 1972 *Phys. Rev. Lett.* **29** 618
- [8] Weigold E, Hood S T and Teubner P J O 1973 *Phys. Rev. Lett.* **30** 475
- [9] Moore J H, Coplan M A, Skillman T L and Brooks E D 1978 *Rev. Sci. Instrum.* **49** 463
- [10] Cook J P D, McCarthy I E, Stelbovics A T and Weigold E 1984 *J. Phys. B* **17** 2329
- [11] Todd B R, Lerner N and Brion C E 1994 *Rev. Sci. Instrum.* **65** 349
- [12] Chen X J, Zhou L X, Zhang X H, Yin X F, Xu C K, Shan X, Wei Z and Xu K Z 2004 *J. Chem. Phys.* **120** 7933
- [13] Deng J K, Li G Q, He Y, Huang J D, Deng H, Wang X D, Wang F, Zhang Y A, Ning C G, Gao N F, Wang Y, Chen X J and Zheng Y 2001 *J. Chem. Phys.* **114** 882
- [14] Wu X J, Chen X J, Chen L Q, Li Z J, Yang X F, Shan X, Zheng Y Y and Xu K Z 2005 *Chin. Phys. Lett.* **22** 1649
- [15] Su G L, Ren X G, Zhang S F, Ning C G, Zhou H, Li B, Huang F, Li G Q and Deng J K 2005 *Acta Phys. Sin.* **54** 4108 (in Chinese)
- [16] Li G Q, Deng J K, Li B, Ren X G, Ning C G, Zhang S F and Su G L 2005 *Acta Phys. Sin.* **54** 466 (in Chinese)
- [17] Zhang S F, Su G L, Ren X G, Ning C G, Zhou H, Li B, Li G Q and Deng J K 2005 *Acta Phys. Sin.* **54** 1552 (in Chinese)
- [18] Brunger M J, McCarthy I E and Weigold E 1999 *Phys. Rev. A* **59** 1245
- [19] Brunger M J and Adcock W 2002 *J. Chem. Soc. Perkin. Trans. 2* **1**

- [20] Storer P, Caprari R S, Clark S A C, Vos M and Weigold E 1994 *Rev. Sci. Instrum.* **65** 2214
- [21] Vos M, Cornish G P and Weigold E 2000 *Rev. Sci. Instrum.* **71** 3831
- [22] Zheng Y, Cooper G, Tizier S, Todd B R and Brion C E 2000 *J. Electron Spectrosc. Relat. Phenom.* **112** 67
- [23] Takahashi M, Saito T, Matsuo M and Udagawa Y 2002 *Rev. Sci. Instrum.* **73** 2242
- [24] Shan X, Chen X J, Zhou L X, Li Z J, Liu T, Xue X X and Xu K Z 2006 *J. Chem. Phys.* **125** 154307
- [25] Takahashi M, Watanabe N, Khajuria Y, Udagawa Y and Eland J H D 2005 *Phys. Rev. Lett.* **94** 213202
- [26] Bawagan A O, Brion C E, Davidson E R and Feller D 1987 *Chem. Phys.* **113** 19
- [27] Ning C G, Ren X G, Deng J K, Su G L, Zhang S F, Knippenberg S and Deleuze M S 2006 *Chem. Phys. Lett.* **421** 52
- [28] Miron C, Simon M, Leclercq N and Morin P 1997 *Rev. Sci. Instrum.* **68** 3728
- [29] Reddish T J, Richmond G, Bagley G W, Wightman J P and Cvejanović S 1997 *Rev. Sci. Instrum.* **68** 2685
- [30] Young D T, Ghielmetti A G, Shelley E G, Marshall J A, Burch J L and Booker T L 1987 *Rev. Sci. Instrum.* **58** 506
- [31] van Boeyen R W and Williams J F 2005 *Rev. Sci. Instrum.* **76** 063303
- [32] Catoire F, Staicu-Casagrande E M, Lahmam-Bennani A, Duguet A, Naja A and Ren X G 2007 *Rev. Sci. Instrum.* **78** 013108
- [33] Ning C G, Ren X G, Deng J K, Su G L, Zhang S F, Huang F and Li G Q 2005 *Chin. Phys.* **14** 2467
- [34] Su G L, Ren X G, Zhang S F, Ning C G, Zhou H, Li B, Li G Q and Deng J K 2005 *Chin. Phys.* **14** 1966
- [35] Ren X G, Ning C G, Deng J K, Zhang S F, Su G L, Huang F and Li G Q 2005 *Chin. Phys. Lett.* **22** 1382
- [36] Yang T C, Ning C G, Su G L, Deng J K, Zhang S F, Ren X G and Huang Y R 2006 *Chin. Phys. Lett.* **23** 1157
- [37] Ning C G, Ren X G, Deng J K, Zhang S F, Su G L, Huang F and Li G Q 2005 *J. Chem. Phys.* **122** 224302
- [38] Jagutski O, Lapington J, Worth L B, Spillman U, Mergel V and Schmidt-Böcking H 2002 *Nucl. Instr. and Meth.* **477** 256
- [39] Ning C G, Deng J K, Su G L, Zhou H and Ren X G 2004 *Rev. Sci. Instrum.* **75** 3062
- [40] Duffy P, Casida M E, Brion C E and Chong D P 1992 *Chem. Phys.* **159** 347
- [41] Jagutzki O, Cerezo A, Czasch A, Dörner R, Hattabaß M, Huang M, Mergel V, Spillmann U, Ullmann-Pfleger K, Weber T, Schmidt-Böcking H and Smith G D W 2002 *IEEE Trans. Nucl. Sci.* **49** 2477
- [42] Ren X G, Ning C G, Deng J K, Zhang S F, Su G L, Huang F and Li G Q 2005 *Phys. Rev. Lett.* **94** 163201
- [43] Cho T K, Takahashi M and Udagawa Y 2006 *J. Photoch. Photobio. A* **178** 281
- [44] Ning C G, Ren X G, Deng J K, Su G L, Zhang S F and Li G Q 2006 *Phys. Rev. A* **73** 022704
- [45] Takahashi M, Saito T, Hiraka J and Udagawa Y 2003 *J. Phys. B At. Mol. Opt. Phys.* **36** 2539
- [46] Knippenberg S, Deleuze M S, Cleij T J, Francois J P, Cederbaum L S and Eland J H D 2005 *J. Phys. Chem. A* **109** 4267
- [47] Knippenberg S, Nixon K L, Brunger M J, Maddern T, Campbell L, Trout N, Wang F, Newell W R, Deleuze M S, Francois J P and Winkler D A 2004 *J. Chem. Phys.* **121** 10525
- [48] Yan B, Pan S F and Yu J H 2007 *Chin. Phys.* **16** 1956
- [49] Li S H, Li R X, Ni G Q and Xu Z Z 2004 *Chin. Phys.* **13** 1009
- [50] Han X Y and Li J M 2006 *Phys. Rev. A* **74** 062711